

# Chitosan-Modified Polyethyleneimine Nanoparticles for Enhancing the Carboxylation Reaction and Plants' CO<sub>2</sub> Uptake

Cyril Routier,<sup>1</sup> Lorenzo Vallan,<sup>2</sup> Yohann Daguerre, Marta Juvany, Emin Istif, Daniele Mantione, Cyril Brochon, Georges Hadziioannou, Åsa Strand, Torgny Näsholm, Eric Cloutet, Eleni Pavlopoulou, and Eleni Stavrinidou\*



Cite This: *ACS Nano* 2023, 17, 3430–3441



Read Online

ACCESS |



Metrics & More



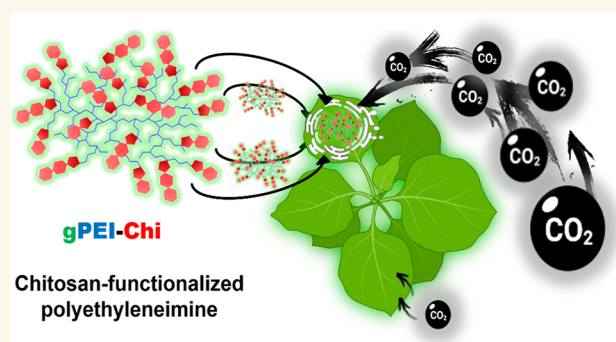
Article Recommendations



Supporting Information

**ABSTRACT:** Increasing plants' photosynthetic efficiency is a major challenge that must be addressed in order to cover the food demands of the growing population in the changing climate. Photosynthesis is greatly limited at the initial carboxylation reaction, where CO<sub>2</sub> is converted to the organic acid 3-PGA, catalyzed by the RuBisCO enzyme. RuBisCO has poor affinity for CO<sub>2</sub>, but also the CO<sub>2</sub> concentration at the RuBisCO site is limited by the diffusion of atmospheric CO<sub>2</sub> through the various leaf compartments to the reaction site. Beyond genetic engineering, nanotechnology can offer a materials-based approach for enhancing photosynthesis, and yet, it has mostly been explored for the light-dependent reactions. In this work, we developed polyethyleneimine-based nanoparticles for enhancing the carboxylation reaction. We demonstrate that the nanoparticles can capture CO<sub>2</sub> in the form of bicarbonate and increase the CO<sub>2</sub> that reacts with the RuBisCO enzyme, enhancing the 3-PGA production in *in vitro* assays by 20%. The nanoparticles can be introduced to the plant *via* leaf infiltration and, because of the functionalization with chitosan oligomers, they do not induce any toxic effect to the plant. In the leaves, the nanoparticles localize in the apoplasmic space but also spontaneously reach the chloroplasts where photosynthetic activity takes place. Their CO<sub>2</sub> loading-dependent fluorescence verifies that, *in vivo*, they maintain their ability to capture CO<sub>2</sub> and can be therefore reloaded with atmospheric CO<sub>2</sub> while *in planta*. Our results contribute to the development of a nanomaterials-based CO<sub>2</sub>-concentrating mechanism in plants that can potentially increase photosynthetic efficiency and overall plants' CO<sub>2</sub> storage.

**KEYWORDS:** nanoparticles, CO<sub>2</sub> capture, polyethyleneimine, chitosan, photosynthesis



During photosynthesis, plants capture carbon dioxide (CO<sub>2</sub>) and, by utilizing light energy, convert it to carbohydrates, which is the energy source of most heterotrophic organisms but also a source of fibers and biofuels. With the growing population, saturation of resources, and the climate crisis, there is a great need to improve plants photosynthetic efficiency and increase crop yield. One of the major limiting steps of photosynthesis occurs during the initial carboxylation reaction for carbon fixation in the chloroplasts. During this step of the Calvin cycle, CO<sub>2</sub> is converted to the organic acid 3-PGA (3-phosphoglycerate) catalyzed by the RuBisCO (Ribulose 1,5-bisphosphate carboxylase/oxygenase) enzyme.<sup>1,2</sup> While RuBisCO has naturally poor affinity for CO<sub>2</sub>,

its dual nature as oxygenase also leads to a competing reaction with O<sub>2</sub>, creating the wasteful pathway of photorespiration that reduces the Calvin cycle's efficiency by decreasing the photosynthetic carbon fixation of more than 25%.<sup>3,4</sup> Furthermore, to reach the RuBisCO enzyme, atmospheric

**Received:** September 16, 2022

**Accepted:** February 10, 2023

**Published:** February 16, 2023



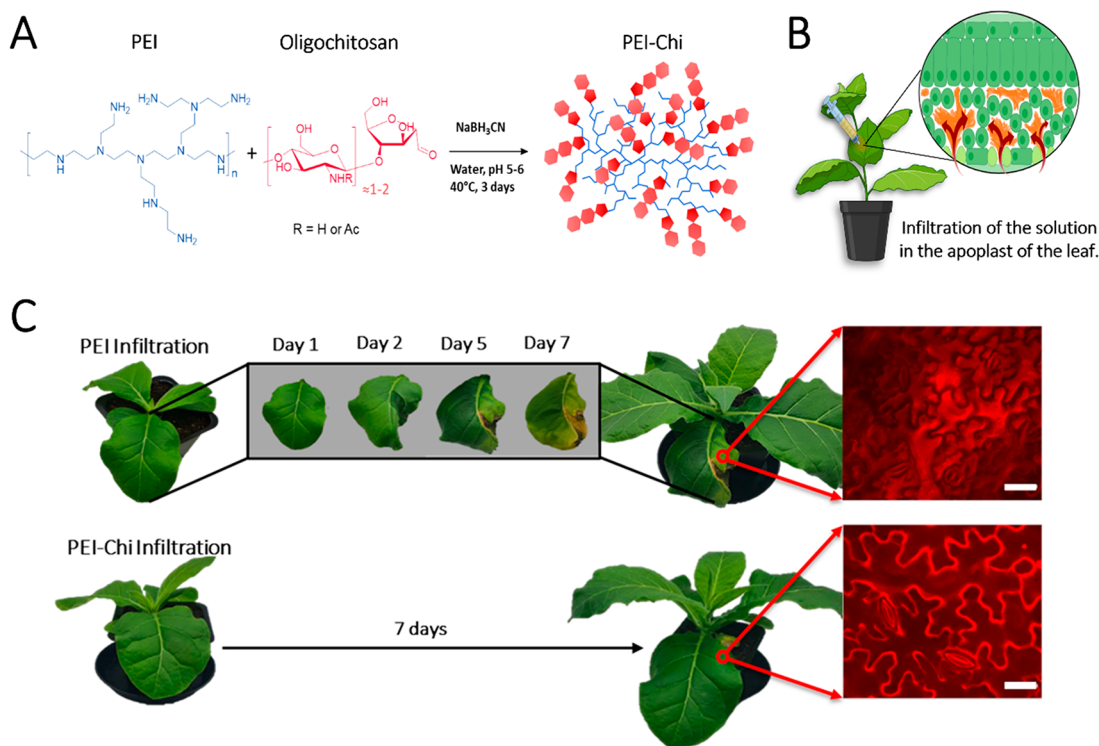


**Figure 1.** Infiltration of PEI-Chi in *Nicotiana tabacum* (tobacco) plants and evaluation of its phytotoxicity (A) Functionalization of PEI with oligochitosan by reductive amination. (B) Scheme of the infiltration method: a solution contained in a needleless syringe is infiltrated in the abaxial part of a leaf by gently applying pressure. The solution is pushed in the intercellular space existing between the cells' membrane called apoplast (created with BioRender.com). (C) Comparison of the effects of the infiltration of PEI (above) and PEI-Chi (below) on the tobacco leaf. PEI infiltration leads to a quick damage in the infiltrated area and around it while the infiltration of PEI-Chi does not show any visible sign of toxicity even one month after infiltration (Figure S14). The insets on the right show fluorescent imaging obtained after staining of the samples with propidium iodide, a cationic dye that does not cross intact membranes but binds to cell walls, forming an outline of living cells. Scale bar: 50  $\mu\text{m}$ .

$\text{CO}_2$  has to follow a resistive pathway and diffuse through the leaf stomata, the intercellular space, the cell membrane, cytoplasm, and finally the chloroplast envelopes.<sup>5,6</sup> Thus, in order to sustain their growth, plants synthesize a large number of RuBisCO enzymes, which requires high nitrogen use, a process that can be problematic for the plant development when nitrogen availability is limited.

Despite great progress in understanding RuBisCO biosynthesis and catalytic action, but also advances on plastid transformation<sup>7</sup> and RuBisCO recombinant expression,<sup>8,9</sup> improving RuBisCO's catalytic activity and specificity to  $\text{CO}_2$  in crop plants via genetic engineering remains a complex and challenging endeavor.<sup>10,11</sup> Apart from direct enzyme engineering, another promising route is to increase the amount of  $\text{CO}_2$  in the vicinity of RuBisCO via a  $\text{CO}_2$ -concentrating mechanism,<sup>12</sup> either biochemically, such as  $\text{C}_4$  photosynthesis<sup>13,14</sup> or through the expression of inorganic carbon transporters such as those for bicarbonate.<sup>15</sup>

Beyond genetic engineering, other approaches to enhance or augment plant functions based on materials science and nanotechnology have emerged.<sup>16–18</sup> Synthetic materials can be rationally designed with desired properties that are optimized independently of the biological environment. However, it is challenging to introduce the synthetic materials into the biological organism in a seamless manner and incorporate the synthetic functionality into the biological machinery. In the literature, several examples at the proof-of-concept level exist. Functionalized nanotubes have been introduced to plants for *in*

*in vivo* detection of endogenous analytes such as  $\text{H}_2\text{O}_2$ <sup>19</sup> or to convert plants to environmental sensors for detecting exogenous analytes such as arsenic.<sup>20</sup> Quantum dots have been used for *in vivo* targeted delivery of biochemicals,<sup>21</sup> while conjugated polymer nanoparticles were used for controlling plant functions via light stimulation.<sup>22</sup> Our group, on the other hand, focused on the development of plant biohybrids using the biochemistry of plants to polymerize *in vivo* conducting polymers that can be used for energy storage.<sup>23–25</sup>

Enhancing photosynthesis with synthetic materials has been attempted by mostly focusing on improving the light-dependent reactions. Semiconducting nanoparticles that localized in the proximity of the thylakoids have shown to improve the electron transport rates<sup>26,27</sup> and/or act as antennas, extending the light absorption spectrum of the plant.<sup>28,29</sup> To date, leveraging nanomaterials for enhancing the  $\text{CO}_2$  uptake of plants has not been demonstrated.

Polyethyleneimine-based materials are promising candidates as they have an excellent  $\text{CO}_2$  capture ability as it was demonstrated by several studies focusing on the design of new  $\text{CO}_2$  absorbents for postcombustion processes.<sup>30–32</sup> The highly dense amines of polyethyleneimine (PEI) react with  $\text{CO}_2$ , forming zwitterionic species such as carbamic acids and carbamates or, in the presence of water, the corresponding ammonium hydrogen carbonate salts. Furthermore, PEI or PEI-coated nanomaterials can cross plant cellular barriers and localize in the cytosol or organelles, as it was demonstrated both *in vitro*<sup>33,34</sup> and *in vivo* studies. Particularly, PEI has been

used as carrier to deliver plasmids to plants for transient gene expression,<sup>35</sup> as well as to deliver small interfering RNA, siRNA, for gene silencing.<sup>36</sup> PEI's high positive charge condensates negatively charged polynucleotides and, at the same time, protects them from degradation, thus improving transfection efficiency. Yasumoto et al. demonstrated that small biogenic polyamines, such as piperazine and putrescine, can capture atmospheric CO<sub>2</sub> which can then be used as a substrate for the carboxylation reaction.<sup>37</sup> However, they have not studied their introduction to plants or their phytotoxicity. Other polyamines, such as PEI, can be highly toxic to plants depending on their molecular structure and concentration used.<sup>38</sup>

In this work, we designed phytocompatible green-fluorescent PEI-based nanoparticles that can capture and transfer CO<sub>2</sub> to RuBisCO for the carboxylation reaction. The phytotoxicity of the nanoparticles is inhibited by the presence of protective chitosan oligomers, while the fluorophore functionalization enables CO<sub>2</sub> loading-dependent fluorescence that does not overlap with the leaf autofluorescence. The nanoparticles were introduced to the plant via infiltration, and they spontaneously localized within the chloroplasts where photosynthesis takes place.

## RESULTS AND DISCUSSION

Branched PEI of 2 kDa molecular weight was chosen as an initial potential candidate for enhancing plants' CO<sub>2</sub> uptake and carbon fixation. However, infiltration of branched PEI in *Nicotiana tabacum* (tobacco) leaves revealed its toxicity for the plant as it will be discussed in detail in the next section. The synthesis of polymers containing both ethylenamide and glycoside units recently proved to be a promising strategy for the preparation of nontoxic gene vectors.<sup>39–41</sup> Inspired by this approach, we modified 2 kDa PEI with chitosan oligomers. Chitosan is obtained from the partial deacetylation of chitin, the constituent of several crustaceans and insects exoskeleton, and therefore, it is the second most abundant polymer in nature after cellulose. As an emerging biocompatible, biodegradable, and cheap material, chitosan and chitosan nanoparticles have found use in several fields, such as packaging,<sup>42</sup> gene delivery,<sup>43</sup> enzyme immobilization,<sup>44</sup> water treatment,<sup>45</sup> and agriculture.<sup>46</sup> Chitosan-based materials have been used in plant applications for enhancing seedling growth,<sup>47</sup> controlled release of nutrients,<sup>48</sup> and for antifungal and antibacterial purposes.<sup>49</sup> First, chitosan oligomers (oligochitosan), of average 2–3 sugar units (Figure S1), were prepared by nitrous acid-promoted depolymerization of chitosan (MW 15 kDa), exploiting a previously reported procedure that allows to roughly control the size of the oligomers through the stoichiometry of the reaction.<sup>50</sup> In contrast with the chitosan polymer, these oligosaccharides are highly soluble in water even at neutral pH. Moreover, the cleavage of the glycosidic linkage during the depolymerization reaction forms a 2,5-anhydro-D-mannofuranose reducing-end, whose aldehyde group does not participate in intramolecular hemiacetals and can be exploited for further reactions. In the second step, we performed a reductive amination reaction between the amines of PEI and the aldehydes of oligochitosans. By forming a C–N covalent bond between PEI and oligochitosan, this synthetic route converts the primary amines of PEI to secondary amines and the secondary amines to tertiary amines. In this way, PEI-Chi was obtained, consisting of a PEI branched molecule covered by numerous

oligochitosan functionalities (Figure 1A). It should be noted that this functionalization strategy does not consume PEI amine groups, thus not reducing the polymer's ability to capture CO<sub>2</sub>. PEI-Chi structure was investigated by nuclear magnetic resonance (NMR) spectroscopy. In the proton (<sup>1</sup>H) and carbon (<sup>13</sup>C) APT (attached proton test) NMR spectra of PEI-Chi, the signals of the oligochitosan and PEI parts are present, whereas the aldehyde signal, located at 5.01 ppm in the <sup>1</sup>H spectrum of oligochitosan, has disappeared in the spectrum of PEI-Chi, demonstrating that the functionalization has taken place (Figures S2–S6). Finally, we labeled PEI-Chi with a small amount of fluorescein isothiocyanate (FITC), whose fluorescence can be exploited for *in vivo* localization studies. By washing with ethanol and acetone, the free dye was completely removed, and we isolated the green-fluorescent PEI-Chi (gPEI-Chi). The NMR spectra of gPEI-Chi showed no significant differences from those of PEI-Chi, except for weak proton signals between 7.7 and 6.5 ppm, which suggest the presence of bound FITC (Figures S7–S9). Infrared spectroscopy (IR) analysis of oligochitosan, PEI-Chi and gPEI-Chi showed the typical vibrational features of polysaccharides (Figure S10). In detail, the spectrum of gPEI-Chi shows wide and multiple absorption bands between 3600 and 3300 cm<sup>-1</sup>, which correspond to O–H and N–H stretching, free or involved in hydrogen bonds. Between 2928 and 2868 cm<sup>-1</sup> it is observed the C–H symmetric and asymmetric stretching of the glycans and PEI skeleton, while the bands at 1649 and 1560 cm<sup>-1</sup> correspond to amide I and amide II vibrational modes. Even N–H bending probably contributes to the intensity of those bands, as features in the same area are present in the spectrum of bare PEI. The signals between 1414 and 1317 cm<sup>-1</sup> were attributed to O–H bending, while C–OH and C–O–C stretching mainly contributes to the peaks located at 1149, 1069, and 1024 cm<sup>-1</sup>. An additional contribution to the absorption in this range is given by the C–N stretching, which also appears in the spectrum of bare PEI at 1117 and 1042 cm<sup>-1</sup>.<sup>51</sup> Atomic force microscopy (AFM) characterization of gPEI-Chi (Figure S11) showed that the sample is composed of individual nanoparticles with 2.0–2.5 nm size and of larger particles, which could consist of aggregates of about 5 nm. For comparison, the individual nanoparticles of bare PEI show an average size of 1.0–1.5 nm, therefore the larger size of gPEI-Chi is due to the oligochitosan functionalization. Size exclusion chromatography (SEC) also confirmed the increase of size, estimating a molecular weight of gPEI-Chi more than doubled with respect to bare PEI (Figure S12 and Table S13). In addition, the dispersity of gPEI-Chi is higher than that of bare PEI as a result of the functionalization.

Next, we proceeded to characterize the phytotoxicity of gPEI-Chi and compared it with bare branched PEI. Both polymers were infiltrated in the apoplast of 6 weeks old *Nicotiana tabacum* (tobacco) leaves (Figure 1B). To maintain cell homeostasis, the materials were dissolved in a typical aqueous buffer used for infiltration, consisting of 2-(N-morpholino)ethanesulfonic acid (MES) (pH 5.6) and MgCl<sub>2</sub>, both in the concentration of 10 mM.<sup>52–54</sup> The plants were visually inspected for a minimum of 7 days after infiltration. As shown in Figure 1C, the leaves infiltrated with bare PEI stopped growing with clear toxicity effects. The infiltrated area dried out and became brittle, while the adjacent tissue exhibited chlorosis. Indeed, it has been found that PEI in PEI-functionalized nanotubes induces transcriptional reprog-

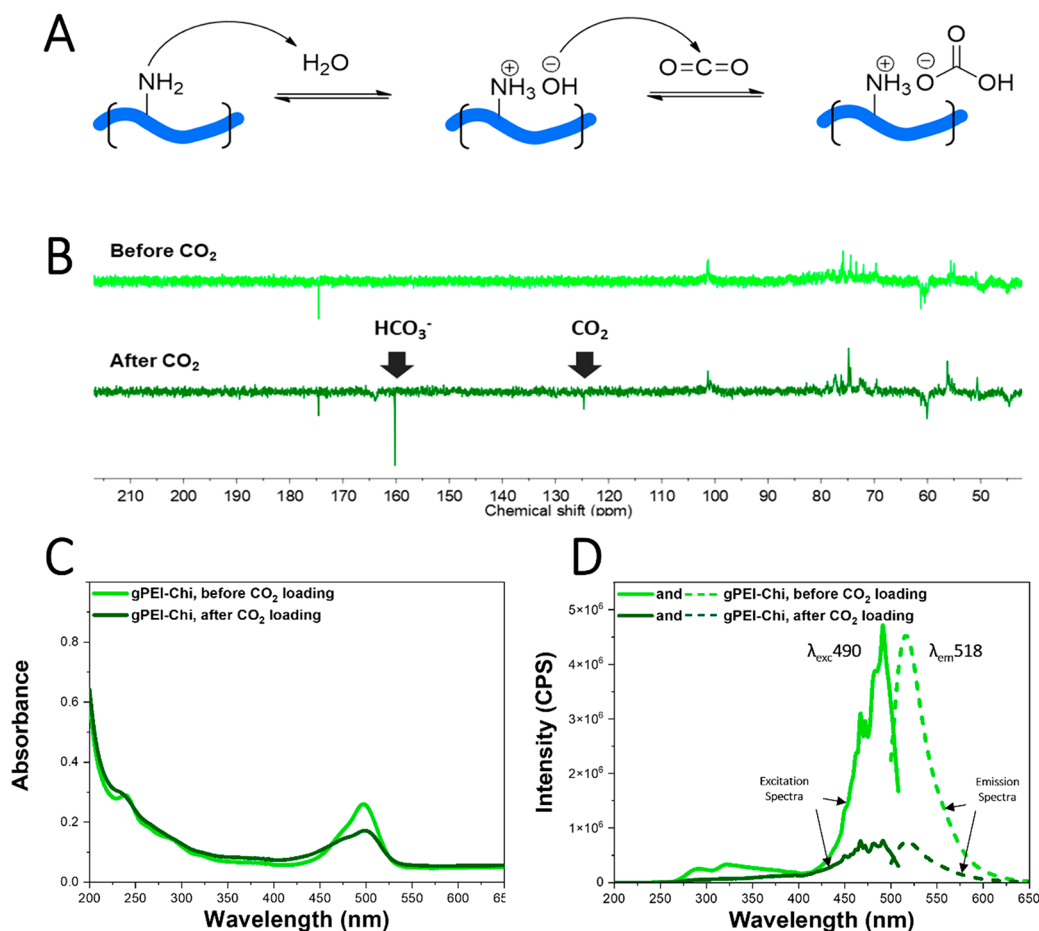


**Figure 2.** Functionalization of PEI-Chi for fluorescent detection *in vivo* and CO<sub>2</sub> uptake emission dependence. (A) Scheme of the ammonium bicarbonate formation from the reaction between amine and CO<sub>2</sub> in aqueous environment (PEI contains primary, secondary, and tertiary amines and all three kinds can react with CO<sub>2</sub>. We here used primary amines only as a showcase). (B) APT NMR spectra of PEI-Chi in D<sub>2</sub>O before and after bubbling carbon dioxide. After bubbling, strong peaks corresponding to hydrogen carbonate and CO<sub>2</sub> appear. (C) Absorption and (D) excitation and emission spectra of gPEI-Chi (0.05 mg/mL) in water before and after saturating the solution with carbon dioxide.

ramming in plants, leading to stress, immune responses, and senescence that may lead to cell death and tissue damage depending on the concentration of PEI and structure.<sup>55</sup>

In contrast, the plants infiltrated with gPEI-Chi did not show any visible sign of toxicity for more than a week and the infiltrated leaves continued to grow normally. To verify the tissue integrity of the infiltrated leaves, we performed histochemical staining with Propidium Iodide (PI). PI is a fluorescent dye that binds to the plant cell wall and cannot cross the intact cell membrane (insets in Figure 1C). The area of leaves infiltrated with PEI could not be stained with PI as it dried out with no intact cells for efficient staining. The adjacent discolored tissue was stained with the dye entering the cells, indicating that the membranes were damaged and the cells dying. Instead, in the case of gPEI-Chi infiltrated leaves, the PI did not cross the cell membranes, not even very close to the infiltration point, indicating that the cells are intact and that the oligochitosan functionalization effectively improved the phytocompatibility of PEI.

The ability of PEI-Chi to bind carbon dioxide and store it in the form of hydrogen carbonate ions was studied by NMR spectroscopy (Figure 2A,B). CO<sub>2</sub> was bubbled in a deuterium oxide solution of PEI-Chi (30 mg/mL) and the carbon APT spectrum was recorded. A strong peak appears at 160 ppm

after CO<sub>2</sub> bubbling, corresponding to the HCO<sub>3</sub><sup>-</sup> anion. A smaller peak at 125 ppm corresponds instead to carbon dioxide, which is in equilibrium with the hydrogen carbonate. The pH of the solution shifted from 8 to 9 to 5–6 after CO<sub>2</sub> bubbling, reflecting the conversion of amines into ammonium hydrogen carbonate groups. The APT experiment was repeated in absence of PEI-Chi under identical experimental conditions, finding that in pure D<sub>2</sub>O no signal of bicarbonate appeared after CO<sub>2</sub> bubbling (Figure S15), thus demonstrating the essential role of PEI-Chi in storing CO<sub>2</sub> as bicarbonate.

Then we investigated the optical properties of gPEI-Chi with UV–vis absorption and fluorescence emission spectroscopy (Figure 2C,D). Fluorescence emission with a maximum at 518 nm was observed for λ<sub>exc</sub> = 490 nm, corresponding to the FITC fluorescence. This emission wavelength is particularly convenient for *in vivo* detection and localization studies as it does not interfere with the plant tissue autofluorescence.

Next, we studied the change in fluorescence due to the CO<sub>2</sub> loading in solution. Interestingly, both absorption and fluorescence decreased significantly after CO<sub>2</sub> loading. We hypothesize that prior to CO<sub>2</sub> bubbling, fluorescein is present as a dianion where both the carboxylic acid and the phenol group are deprotonated due to the strong basic environment generated by the abundant surrounding amines of the gPEI-

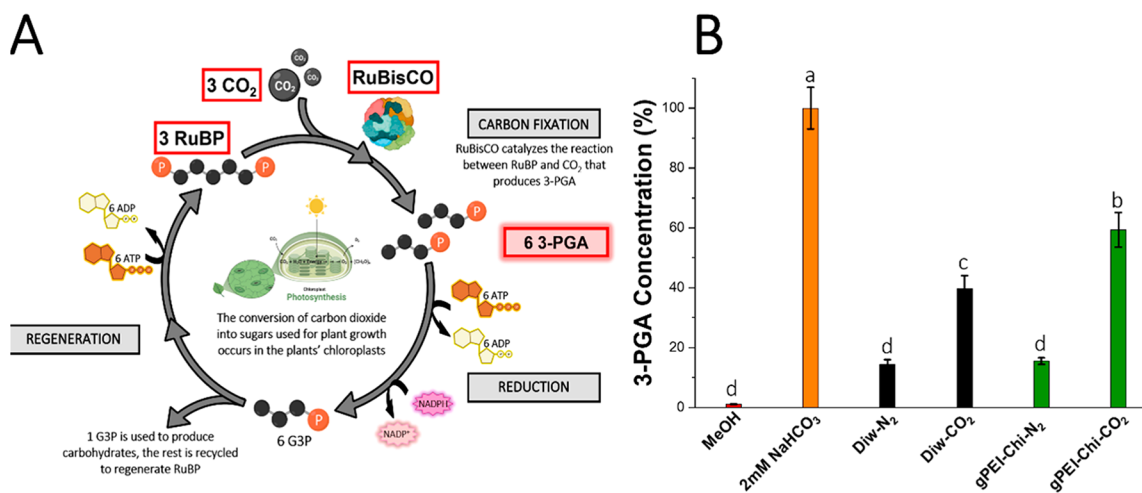


**Figure 3.** Evaluation of 3-phosphoglycerate production using gPEI-Chi as a CO<sub>2</sub>-giver to activate RuBisCO. (A) Simplified Calvin cycle showing the importance of RuBisCO as catalyst for the conversion of RuBP to 3-PGA using CO<sub>2</sub> (created with BioRender.com). (B) Either CO<sub>2</sub> gas or N<sub>2</sub> gas, to remove CO<sub>2</sub>, was bubbled for 30 min in 10 mL of either 1 mg/mL of gPEI-Chi or distilled water. The solutions loaded with CO<sub>2</sub> were then used as substrates for the carboxylation reaction between RuBP and CO<sub>2</sub> catalyzed by RuBisCO and compared to their equivalent without CO<sub>2</sub> treatment and to NaHCO<sub>3</sub> (2 mM) as a carbon source for positive control. The amount of 3-PGA produced by the reaction was then analyzed by LC-MS. Bars indicate the standard errors ( $n = 3$ ). Treatments not labeled by the same letter are significantly different. Tukey-Kramer HSD,  $P$ -value < 0.001. JMP Pro software was used to run the analysis.

Chi structure. When gPEI-Chi reacts with carbon dioxide, the pH of the solution decreases and the phenol is restored, causing a loss of emission intensity since the monoanion form has a lower quantum yield compared to the dianion form.<sup>56</sup>

The decrease in fluorescence intensity due to CO<sub>2</sub> loading was observable even when we used the infiltration buffer as the solvent, indicating that even local pH changes induce a change in the nanoparticles' fluorescence (Figure S16). The CO<sub>2</sub>-dependent fluorescence of gPEI-Chi is very promising for *in vivo* studies as it may enable monitoring CO<sub>2</sub> concentration dynamics, providing insight on the CO<sub>2</sub> uptake and transport within the leaf.

After validating the ability of gPEI-Chi to uptake CO<sub>2</sub>, we proceeded to investigate whether the loaded CO<sub>2</sub> can participate in biochemical reactions and specifically the carboxylation reaction. During this first phase of the Calvin cycle, CO<sub>2</sub> reacts with the RuBisCO, which converts ribulose-1,5-bisphosphate (RuBP) into 3-phosphoglycerate (3-PGA) (Figure 3A).<sup>57</sup>

CO<sub>2</sub> is electrostatically bound to PEI-Chi in the form of hydrogen carbonate which cannot react directly with RuBisCO. However, CO<sub>2</sub> and hydrogen carbonate exist in thermodynamic equilibrium, and they dynamically interchange through reaction with water. We hypothesize that PEI-Chi will increase the hydrogen bicarbonate concentration and consequently the amount of CO<sub>2</sub> available for RuBisCO. The ability of RuBisCO to use the CO<sub>2</sub> delivered by PEI-Chi as substrate for the synthesis of 3-PGA *in vitro* was evaluated with an enzymatic assay adapting the method previously described by Yasumoto *et al.*<sup>57</sup> We evaluated the activity of RuBisCO in five different aqueous solutions: gPEI-Chi in water (1 mg/mL) bubbled with N<sub>2</sub> (gPEI-Chi-N<sub>2</sub>) or CO<sub>2</sub> (gPEI-Chi-CO<sub>2</sub>), deionized water (DIw) bubbled with N<sub>2</sub> (DIw-N<sub>2</sub>), or CO<sub>2</sub> (DIw-CO<sub>2</sub>) as negative controls, and 2 mM NaHCO<sub>3</sub> as positive control.

These solutions were added in a buffered solution with RuBisCO and were let to incubate for 10 min at room temperature in order to activate the enzyme. Next, RuBP was

introduced, triggering the RuBisCO/CO<sub>2</sub> catalyzed synthesis of 3-PGA. After 6 min, the reaction was stopped by addition of formic acid. Finally, the 3-PGA concentration in each solution was quantified with liquid chromatography-mass spectrometry (LC-MS) and normalized so that the amount of 3-PGA produced by the positive control NaHCO<sub>3</sub> correspond to 100%. As shown in Figure 3B, the concentration of 3-PGA was 45% higher in the gPEI-Chi-CO<sub>2</sub> solution compared to the gPEI-Chi-N<sub>2</sub>. Furthermore, the 3-PGA concentration in the gPEI-Chi-CO<sub>2</sub> solution was 20% higher than in DIw-CO<sub>2</sub>, verifying that gPEI-Chi-CO<sub>2</sub> can effectively increase the CO<sub>2</sub> amount that reacts with RuBisCO via the hydrogen carbonate -CO<sub>2</sub> conversion in water. When 2 mM NaHCO<sub>3</sub> was used, the concentration of 3-PGA produced by RuBisCO was higher than that produced in the presence of gPEI-Chi, probably due to different concentration of captured CO<sub>2</sub>. However, in contrast to gPEI-Chi, NaHCO<sub>3</sub> cannot be infiltrated in plants as it is highly toxic. Thus, these results suggest that gPEI-Chi could potentially improve the CO<sub>2</sub> conversion of the plant by increasing the CO<sub>2</sub> concentration in the RuBisCO environment.

After demonstrating the ability of gPEI-Chi to efficiently increase the CO<sub>2</sub> that reacts with RuBisCO *in vitro*, we investigated the localization of the nanoparticles in the leaf tissue to gain insight on their potential for reaching the chloroplasts and increasing the CO<sub>2</sub> amount at the photosynthetic sites *in vivo*. According to the lipid exchange envelope penetration (LEEP) model, infiltrated nanoparticles can spontaneously localize in the chloroplast depending on their size and surface charge. Nanoparticles must be within a specific range of size and zeta potential, to penetrate the negatively charged membrane of the chloroplasts and localize within their stroma.<sup>58</sup> We quantified the  $\zeta$ -potential of the gPEI-Chi nanoparticles in the aqueous infiltration buffer (pH 5.6) and found a small shift from 35.8 mV before CO<sub>2</sub> bubbling to 37.4 mV after. The size and  $\zeta$ -potential distributions, and possibility of aggregation of the nanoparticles, at the pH used for infiltration, indicate that some of the nanoparticles may

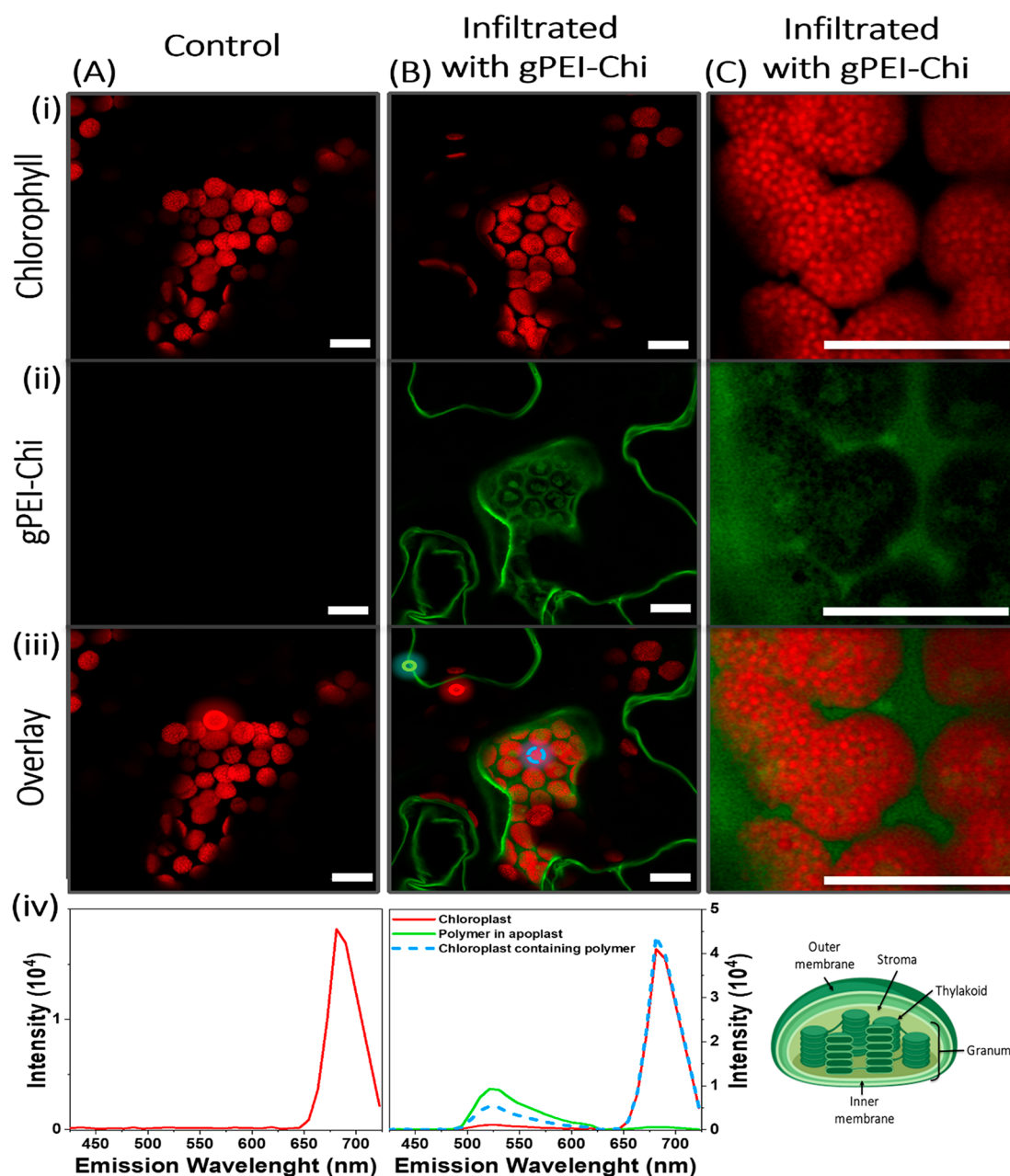


**Figure 4.** Confocal microscopy imaging to evaluate the chloroplast accessibility to gPEI-Chi-CO<sub>2</sub>. Imaging of column (A) a control tobacco leaf, column (B) and (C) a leaf infiltrated with gPEI-Chi-CO<sub>2</sub>. The top red panel (i) shows the autofluorescence of the chlorophyll, the middle green panel (ii) shows the gPEI-Chi-CO<sub>2</sub> fluorescence, and the panel (iii) is a merging of the two previous. The graphs (A-iv) and (B-iv) are emission spectra of the circles in the merged images, obtained with a monochromator, and serve to evaluate the spatial distribution of the gPEI-Chi-CO<sub>2</sub> nanoparticles in respect to the chlorophyll. The schematic (C-iv) represents the structure of a chloroplasts containing thylakoids forming stacks of disks (grana), which are the sites of photosynthetic reactions and contain the chlorophyll (created with BioRender.com). Scale bar: 10  $\mu\text{m}$ .

passively enter the chloroplasts according to the LEEP model (Figure S17). We infiltrated CO<sub>2</sub> loaded gPEI-Chi (gPEI-Chi-CO<sub>2</sub>) in tobacco leaves and, using confocal microscopy, we observed that the nanoparticles mainly localized in the leaf apoplast but could also penetrate the mesophyll cells in the infiltrated area and reach the chloroplasts (Figure 4). The colocalization of the gPEI-Chi-CO<sub>2</sub> nanoparticles and chloroplasts was confirmed by recording the emission spectra of the selected regions (Figure 4A-iv,B-iv) and by calculating the Pearson and Mander's colocalization coefficients (Figure S18). Furthermore, we could observe that the fluorescence of

gPEI-Chi-CO<sub>2</sub> followed the patterns of the discs stacks (grana) formed by the thylakoids inside the chloroplasts, which are the sites of photosynthetic reactions containing the chlorophyll which appear as the fluorescent red dots in the microscopy images (Figure 4C-iv). The confocal imaging confirms that the CO<sub>2</sub>-loaded nanoparticles can reach the photosynthetic sites and thus have the potential to increase the local CO<sub>2</sub> concentration at the RuBisCO site and enhance the carboxylation reaction. In addition, we performed transmission electron microscopy (TEM) imaging of chloroplasts from plants infiltrated with gPEI-Chi-CO<sub>2</sub> and found indications of

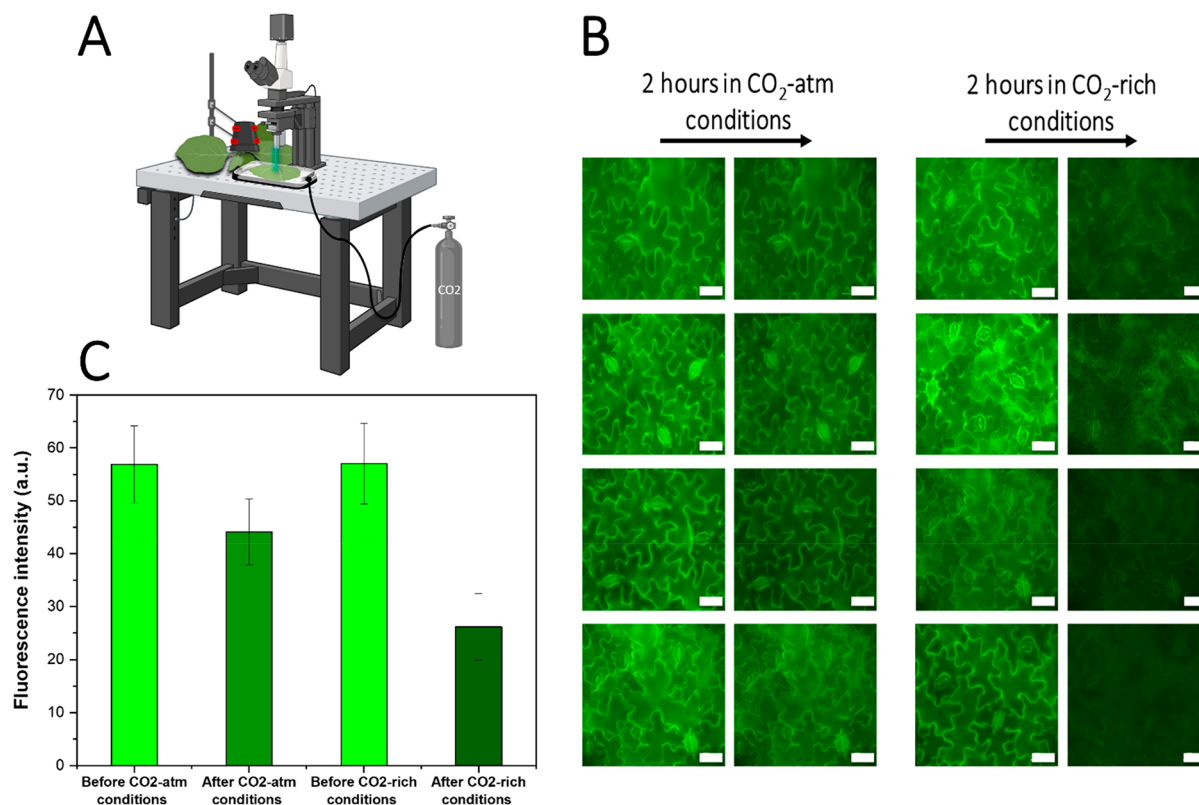


**Figure 5.** *In vivo* CO<sub>2</sub> uptake of gPEI-Chi. (A) Scheme of the experimental setup where a leaf, still attached to its plant, is isolated in a CO<sub>2</sub> incubator and imaged with fluorescence microscopy (created with BioRender.com). (B) Fluorescence microscopy of *Nicotiana tabacum* (tobacco) leaves infiltrated with gPEI-Chi, with or without incubation in a CO<sub>2</sub>-rich environment for 2 h, ( $n = 4$  plants in each condition). Scale bar: 50  $\mu\text{m}$ . (C) Fluorescence intensity evolution under atmospheric CO<sub>2</sub> conditions or in a CO<sub>2</sub>-rich environment. Bars indicate the standard errors ( $n = 4$  plants).

the internalization of the nanoparticles in the chloroplasts, especially in the starch grains and around the stromal thylakoids (Figure S19).

We then assessed whether the unloaded nanoparticles can uptake CO<sub>2</sub> after infiltration to the plant as this will enable the reloading of the nanoparticles with atmospheric CO<sub>2</sub> and the formation of a sustainable CO<sub>2</sub>-concentrating mechanism in planta. We first infiltrated both N<sub>2</sub>-bubbled and CO<sub>2</sub>-loaded gPEI-Chi in the apoplast of tobacco leaves (Figure S20) and confirmed that gPEI-Chi fluorescence maintained its CO<sub>2</sub> dependence in the *in vivo* environment, i.e., gPEI-Chi fluorescence decreases when it is CO<sub>2</sub>-loaded. Next, to study the capacity of the nanoparticles to capture atmospheric CO<sub>2</sub> while in the leaves, we infiltrated gPEI-Chi previously bubbled with N<sub>2</sub> and then monitored the leaves fluorescence over time. The plants were imaged 1 day after infiltration to let any excessive infiltrated solvent to evaporate. The infiltrated leaves, still attached to the plant, were placed in a CO<sub>2</sub>-rich environment under a fluorescent microscope (Figure 5A) and the change in fluorescence intensity was evaluated after 2 h. As a control, we imaged infiltrated leaves that remained in atmospheric conditions. Figure 5B and C show that the fluorescence intensity decreased 54% for the leaves exposed to high CO<sub>2</sub> concentration in comparison to decrease of 22% for the leaves left in atmospheric conditions, indicating that the nanoparticles in the apoplast of the plant are able to capture CO<sub>2</sub>. The small decrease in intensity in the control sample could also indicate that the nanoparticles can capture some CO<sub>2</sub> when placed in atmospheric conditions, however, there is

also the possibility of photobleaching of the dye after repetitive measurements at the same location. Furthermore, we measured the assimilation rate of infiltrated leaves at saturating light (A: the rate of CO<sub>2</sub> uptake per unit time per unit leaf area ( $\mu\text{mol of CO}_2 \text{ m}^{-2} \text{ s}^{-1}$ )) and at different CO<sub>2</sub> levels using the LI-6800 portable photosynthesis system and found that the infiltrated areas show higher CO<sub>2</sub> uptake than controls 2 days after the infiltration (Figure S21). While these results are promising, more studies beyond the scope of this work are required to prove that the nanoparticles enhance plants photosynthetic activity *in vivo*.

## CONCLUSIONS

In conclusion, we designed chitosan-modified polyethyleneimine nanoparticles, gPEI-Chi, which can capture atmospheric CO<sub>2</sub> in the form of bicarbonate and increase the CO<sub>2</sub> that reacts with RuBisCO enzyme enhancing the carboxylation reaction by 20% in *in vitro* assay. The gPEI-Chi nanoparticles were infiltrated in tobacco leaves and, even after an extended period of time, they did not cause any adverse effect to the plant as PEI's toxicity was obviated by the conjugated oligochitosan moieties. The CO<sub>2</sub>-loaded nanoparticles localized within the extracellular space, but most importantly, they could also pass cellular barriers and localize within the chloroplast organelles, which are the sites of photosynthetic activity. Using the gPEI-Chi CO<sub>2</sub>-dependent fluorescence, we also demonstrated the nanoparticles' ability to uptake CO<sub>2</sub> *in vivo* when the leaf is placed in a CO<sub>2</sub>-rich environment while, in future studies, the fluorescence modulation can be extended

to monitor internal CO<sub>2</sub> concentrations. Overall, our results show that **gPEI-Chi** is a promising nanobiotechnological approach for integrating a CO<sub>2</sub>-concentrating mechanism in plants. CO<sub>2</sub>-loaded nanoparticles could potentially increase the CO<sub>2</sub> concentration in the vicinity of the RuBisCO and then be reloaded by atmospheric CO<sub>2</sub> when in planta. Furthermore, plants possess the carbonic anhydrase enzyme that converts bicarbonate to CO<sub>2</sub>, which can potentially increase the contribution of the **gPEI-Chi**-loaded nanoparticles since the conversion of bicarbonate to CO<sub>2</sub> will be accelerated.<sup>59,60</sup> However, to demonstrate the nanoparticles potential in planta, it will require their extended distribution throughout the plant's photosynthetic sites. Although leaf infiltration is commonly used for introducing materials to plant leaves, the materials are usually distributed close to the infiltration site. Using vacuum infiltration in a detached leaf, we observed an extended distribution of the nanoparticles in the whole leaf area (Figure S22). Still, this method cannot be applied to intact plants apart from small seedlings that can fit into a vacuum chamber.<sup>61,62</sup> Therefore, to evaluate the effect of the **gPEI-Chi** nanoparticles on RuBisCO activity and photosynthetic efficiency *in vivo*, another strategy for extended distribution of the nanoparticles to the plant photosynthetic sites has to be developed such as uptake via root or foliage.

## EXPERIMENTAL SECTION

**Synthesis of Oligochitosan.** For this, 3.0 g of chitosan (MW = 15 kDa, deacetylation degree = 85%, Polysciences) was added to 150 mL of ultrapure water. Then 1.8 mL of HCl 37% was added and the mixture was stirred for 1 h until complete dissolution of the material. Afterward, 800 mg of NaNO<sub>2</sub> was added and immediate N<sub>2</sub> gas evolution was observed. After 16 h, the pH was neutralized with AmberLite IRN78 OH. After filtration, the addition of acetone (300 mL) and centrifugation (8000 rpm, 5 min) allowed the recovery of the chitosan oligomers (oligochitosan). The material was redispersed in a minimum amount of water, precipitated again by acetone addition, and collected by centrifugation. Finally, it was washed with methanol and with acetone. After vacuum-drying, 1.8 g of oligochitosan in the form of a white powder was obtained.

**Synthesis of PEI-Chi.** In a round-bottom flask, 200 mg of branched polyethyleneimine (MW = 2 kDa, Polysciences) was dissolved in 30 mL of 1.5% acetic acid solution in water (v/v); then 600 mg of oligochitosan was added and the stirring solution was heated up to 40 °C. Three separate additions of sodium cyanoborohydride of 150 mg each were performed after 1 h, 6 h, and 24 h. After 3 days, the solution was poured in a larger vessel, 1 mL of triethylamine was added first, and then, after 10 min stirring, 60 mL of acetone, achieving the precipitation of **PEI-Chi**. The solid was recuperated by centrifugation (8000 rpm, 5 min); thus, it was redispersed in a minimum amount of water, precipitated again by acetone addition, and collected by centrifugation. Finally, it was washed with methanol and with acetone. After vacuum-drying, 540 mg of **PEI-Chi** in the form of a beige powder was obtained.

**Functionalization of PEI-Chi with Fluorescein 5-isothiocyanate.** In a round-bottom flask, 130 mg of **PEI-Chi** was dispersed in 50 mL of water, followed by the addition of 0.3 mL of triethylamine. A second solution was prepared by dissolving 5 mg of fluorescein 5-isothiocyanate in 10 mL of dimethyl sulfoxide. Then the fluorescein solution was added slowly to the **PEI-Chi** solution while stirring. After 1 day, **gPEI-Chi** was precipitated by the addition of acetone. The product was collected by centrifugation and washed with a mixture of acetone/ethanol 2:1, where free fluorescein is highly soluble. When no more fluorescein was detected in the supernatant, the precipitate was washed with acetone only and, after vacuum-drying, 96 mg of **gPEI-Chi** in the form of an orange powder was obtained.

**NMR Spectra.** NMR spectra were recorded at 298 K with a 400.33 MHz Bruker Advance spectrometer. Deuterated solvents and NMR

tubes were purchased from Eurisotop. Branched polyethyleneimine (MW 2 kDa) and Chitosan (MW 15 kDa, deacetylation degree 85%) were purchased from Polysciences. Sodium cyanoborohydride (95%), sodium nitrite (97%), triethylamine (99.5%), acetic acid (glacial, 99%) were purchased from Sigma-Aldrich. Fluorescein 5-Isothiocyanate (isomer I, 97%) was purchased from TCI.

**Size Exclusion Chromatography.** Acetic acid aqueous solution was used as the mobile phase at a flow rate of 1.00 mL/min and glycerol as a flow rate marker. All polymers were injected (100 μL of solution) at a concentration of 5 mg/mL after filtration through a 0.45 μm pore-size membrane. The separation was carried out on two Agilent columns [2 × PLgel 5 μm Mixed C (300 × 7.5 mm)] and a guard column (PL gel 5 μm). Columns and detectors were maintained at 40 °C. Relative Mw was determined thanks to a conventional calibration obtained with polyethylene glycol narrow standards.

**UV-vis/NIR Absorption Spectra.** UV-vis/NIR absorption spectra were obtained using an Agilent Cary 5000 instrument. Spectra were recorded between 200 and 800 nm, using a 10 mm side quartz cuvette. The absorption spectra were measured both before and after CO<sub>2</sub> loading of the nanoparticles. The loading was carried out by gently bubbling carbon dioxide through a needle plunged in the polymer water solutions for 5 min.

**Steady-State Fluorescence.** Steady-state fluorescence measurements were carried out with a Horiba FluoroMax 4 spectrofluorimeter using a 10 mm side quartz cuvette. The excitation and emission spectra were measured both before and after CO<sub>2</sub> loading of the nanoparticles. The loading was carried out by gently bubbling carbon dioxide through a needle plunged in the polymer water solutions for 5 min.

**Fourier Transform Infrared Spectroscopy.** Fourier transform infrared spectroscopy (FTIR) measurements were performed on a Nicolet iS 5N FTIR spectrometer. Spectra were collected from 4000 to 400 cm<sup>-1</sup> with the following settings: 16 scans per sample, and spectral resolution: 4 cm<sup>-1</sup>.

**Atomic Force Microscopy.** Atomic force microscopy (AFM) (Dimension Fast Scan, Bruker) was used in a tapping mode using a silicon cantilever (Fastscan-A) with a nominal tip radius of 5 nm. The samples were prepared by drop-casting solution of polymer (0.1 mg/mL, 3000 pm, 120 s) on a mica substrate, which was subsequently dried at room temperature for 1 day and on a hot plate at 60 °C for 5 min.

**ζ-Potential Measurements.** ζ-potential measurements were determined using a Zetasizer (NanoZS90, Malvern, United Kingdom). First, nanoparticles were suspended in morpholino-ethanesulfonic acid (MES, Sigma-Aldrich) (pH 5.6 adjusted with KOH) and the nanoparticle surface charge was determined using zeta potential measurement (averaged over 10 measurements each one having 20 runs).

**Plant Material and Growth Condition.** *Nicotiana tabacum* SRI (tobacco) seeds were sown in the soil and grown in a growth chamber (Percival, CLF PlantClimatics GmbH, Werten, Germany) at 120 μmol m<sup>-2</sup> s<sup>-1</sup> light intensity, 60% relative humidity, and a 12/12 h day/night regime at 24 °C during the day and 18 °C during nighttime. All experiments and measurements were performed using 6 weeks old plants.

**Infiltration of *Nicotiana tabacum* (Tobacco).** Plants were illuminated with light of high intensity of ~500 μmol m<sup>-2</sup> s<sup>-1</sup> for 1 h to make sure the stomata are open. Then, a small hole was made on the abaxial side of the tobacco leaf with the tip of a sterile 0.8 × 50 mm HENKE-JECT syringe needle (1 hole per leaf infiltrated). It is important to note that the hole does not completely puncture through the leaf but only passes the epidermal layer in order to facilitate the infiltration of the solution in the plant tissue. Once the hole was made, 200–300 μL of a 0.1 mg/mL **gPEI-Chi** solution in 10 mM MES, 10 mM MgCl<sub>2</sub>, pH 5.6 (or just 10 mM MES, 10 mM MgCl<sub>2</sub>, pH 5.6 as control) was infiltrated from the hole with a 1 mL needleless syringe. In order to control the applied pressure and not to destroy the plant tissue, the researcher put their finger on the adaxial side of the leaf to maintain in place the syringe on the abaxial side of the leaf and then

by gently pushing the plunger of the syringe to infiltrate the solution in the leaf. Any solution administered on the surface of the leaf was rinsed with water and dried gently with a piece of clean tissue. For microscopy experiments, the infiltrated plants were let to stand 24 to 48 h postinfiltration in normal growth conditions to allow remaining solvent to evaporate, while for toxicity experiments and staining they were let to stand in normal growth conditions up to 1 to 2 weeks.

**Propidium Iodide Staining.** Propidium iodide staining was performed by cutting, with a clean razor blade, the leaf of interest and dipping in for 20 min in a 20  $\mu\text{mol}$  aqueous solution of propidium iodide (Sigma-Aldrich, St. Louis, MO, USA) in a 50 mL conical tube (Sarstedt, Nümbrecht, Germany). The leaf was then removed from the solution and excess staining was removed by rinsing in water. The stained leaves were then directly used for microscopy.

**Fluorescence Microscopy.** Widefield fluorescence imaging was performed with a Ni-E Upright Motorized Microscope (Nikon) equipped with a Zyla sCMOS camera (Andor Technology). The source of illumination was a Lambda DG-4 ultrahigh speed wavelength switching illumination system (Sutter Instrument). The Propidium Iodide emission was detected between 580 and 650 nm using a TRITC filter, a 50 $\times$ /0.60 TU PLAN ELWD objective and an exposure time of 1 s. The gPEI-Chi emission was detected between 510 and 560 nm using a FITC filter, a 50 $\times$ /0.60 TU PLAN ELWD objective and an exposure time of 200 ms. The images were treated using the software NIS-Elements (Nikon) and ImageJ. The samples used for microscopy were prepared by cutting a small leaf section of the infiltrated or stained leaf tissue and inserting it between a glass slide (VWR international GmbH, Darmstadt, Germany) and Menzel-Gläzer coverslip (VWR international GmbH, Darmstadt, Germany) using a 30% glycerol aqueous solution as mounting medium to keep the sample moisturized during imaging.

**RuBisCO Assays.** The enzymatic assays for determining the activity of RuBisCO were realized following the method described by Yasumoto *et al.*<sup>37</sup> The chemicals were purchased from Sigma-Aldrich (St. Louis, MO, USA).

**3-Phosphoglyceric Acid Determination by LC-MS.** 3-Phosphoglyceric acid determination by LC-MS was performed at the Swedish Metabolomics Center in Umeå, Sweden. Before the analysis, 200  $\mu\text{L}$  of freeze-dried sample was resuspended in 50 + 50  $\mu\text{L}$  methanol and water. The chromatographic separation was performed on an Agilent 1290 Infinity UHPLC-system (Agilent Technologies, Waldbronn, Germany). One  $\mu\text{L}$  of each sample were injected onto an Atlantis Premier BEH-HILIC, 1.7  $\mu\text{m}$ , 2.1  $\times$  50 mm<sup>2</sup>, held at 40 °C. The gradient elution buffers were composed of (A) 10 mmol/L ammonium acetate in water of pH 9 and (B) 10 mmol/L ammonium acetate in 10/90 water/acetonitrile (v/v) of pH 9 (pH of aqueous buffer before mixing with methanol). Ammonium hydroxide was used to adjust pH of the mobile phase. A final 5  $\mu\text{M}$  concentration of methylenediphosphonic acid was spiked into the solvents for the analysis. The flow rate was 0.35 mL/min, and the compounds were eluted with a linear gradient consisting of 95–30% B over 7 min, B was held at 30% for 2 min; B was increased to 95% for 0.5 min and held for 1.5 min, then the flow-rate was increased to 0.6 mL min<sup>-1</sup> for 1.5 min; these conditions were held for 0.2 min, after which the flow-rate was reduced to 0.35 mL min<sup>-1</sup> for 0.1 min before the next injection.

The compounds were detected with an Agilent 6546 Q-TOF mass spectrometer equipped with a jet stream electrospray ion source operating in negative ion mode. A reference interface was connected for accurate mass measurements; the reference ions purine (4  $\mu\text{M}$ ) and HP-0921 (Hexakis(1H, 1H, 3H-tetrafluoropropoxy)-phosphazine) (1  $\mu\text{M}$ ) were infused directly into the MS at a flow rate of 0.05 mL min<sup>-1</sup> for internal calibration, and the monitored ions were purine  $m/z$  119.03632; HP-0921  $m/z$  966.000725. The gas temperature was set to 150 °C, the drying gas flow to 8 L min<sup>-1</sup> and the nebulizer pressure 35 psig. The sheath gas temp was set to 350 °C and the sheath gas flow 11 L min<sup>-1</sup>. The capillary voltage was set to 4000 V. The nozzle voltage was 300 V. The fragmentor voltage was 120 V, the skimmer 65 V and the OCT 1 RF Vpp 750 V. The collision energy was set to 0 V. The  $m/z$  range was 70–1700, and data

was collected in centroid mode with an acquisition rate of 4 scans s<sup>-1</sup> (1977 transients/spectrum). Data were processed and analyzed using MassHunter Qualitative Analysis, Quantitative Analysis (QqQ; Agilent) and Excel (Microsoft) software.

Methanol, HPLC-grade, was obtained from Fischer Scientific (Waltham, MA, USA) Acetonitrile, HPLC-grade was obtained from Fischer Scientific (Waltham, MA, USA) 2-Propanol, HPLC-grade was obtained from VWR (Radnor, PA, USA) H<sub>2</sub>O, Milli-Q, Ammonia solution, 35% HPLC-grade was obtained from Fischer Scientific (Waltham, MA, USA). Reference and tuning standards: Purine, 4  $\mu\text{M}$ , Agilent Technologies (Santa Clara, CA, USA) HP-0921 (Hexakis(1H, 1H, 3H-tetrafluoropropoxy)phosphazine), 1  $\mu\text{M}$ , Agilent Technologies (Santa Clara, CA, USA) Calibrant, ESI-TOF, ESI-L Low Concentration Tuning Mix, Agilent Technologies (Santa Clara, CA, USA) HP-0321 (Hexamethoxyphosphazine), 0.1 mM, Agilent Technologies (Santa Clara, CA, USA).

**Confocal Microscopy Imaging.** Confocal imaging was performed with an inverted Zeiss LSM 980 (Carl Zeiss AG, Oberkochen, Germany) confocal microscope equipped with an Airyscan2 detection unit. The objective Plan-Apochromat 63 $\times$ /1.4 Oil DIC M27 (FWD = 0.19 mm, Carl Zeiss AG, Oberkochen, Germany) was used, with Immersol 518 F immersion media ( $n = 1.518$ , Carl Zeiss AG, Oberkochen, Germany) and all images were processed with the Zen Blue software 3.4.

We evaluated the contribution of the polymer at each wavelength using the LSM lambda scan spectrophotometer, and compared images of the green and red channels by using both the confocal and the Airyscan2 super-resolution modes. We captured images in 16 bits with a bidirectional acquisition, an averaging of 4 images, an image size of 1863  $\times$  1863 pixels (pixel size = 0.043  $\mu\text{m}$ ) and a zoom of 1.3. Both the fluoresceine isocyanate (FITC) and chlorophyll were excited using a 488 nm laser at an intensity of 0.4% with a pinhole of 5 AU, a detector gain at 700 V and a pixel time of 1.13  $\mu\text{s}$ . The Alexa Fluorophore 520 (emission wavelength 520 nm) emission filter was used for the detection of gPEI-Chi, and the Alexa Fluorophore 700 (emission wavelength 719 nm) emission filter was used for the detection of the chlorophyll. The samples used were prepared by cutting a small leaf section of tobacco tissue infiltrated with gPEI-Chi preliminary loaded with CO<sub>2</sub> (gPEI-Chi-CO<sub>2</sub>) and inserting it between a glass slide (VWR international GmbH, Darmstadt, Germany) and Menzel-Gläzer coverslip (VWR international GmbH, Darmstadt, Germany) using a 30% glycerol aqueous solution as mounting medium to keep the sample moisturized during imaging. We gently removed via capillarity the extra mounting medium between the glass slide and the coverslip in order to create a suction effect that allows to turn the samples upside down for imaging with the inverted microscope.

**CO<sub>2</sub> Incubation.** Twenty-four to forty-eight hours postinfiltration with gPEI-Chi, the plants were fixed upside down on the fluorescent microscope platform and the infiltrated leaf was isolated in a closed Petri dish having an entry tube for CO<sub>2</sub> and a small hole allowing air circulation. The fluorescence of gPEI-Chi was first imaged in atmospheric conditions; then we filled the Petri dish with CO<sub>2</sub> (coming from a CO<sub>2</sub> tank) for 2 h and captured the fluorescence again.

## ASSOCIATED CONTENT

### Supporting Information

The Supporting Information is available free of charge at <https://pubs.acs.org/doi/10.1021/acsnano.2c09255>.

Figures giving additional details on material investigation including NMR, HSQC, IR spectroscopy, AFM, and SEC; confocal microscopy images investigating long-term toxicity, detectability, and colocalization with chloroplasts *in vivo*; transmission electron microscopy of infiltrated samples; emission spectra and fluorescence microscopy to study CO<sub>2</sub>-dependent fluorescence of

nanoparticles; assimilation-CO<sub>2</sub> response curves of infiltrated plants (PDF)

## AUTHOR INFORMATION

### Corresponding Author

Eleni Stavrinidou – Laboratory of Organic Electronics, Department of Science and Technology, Linköping University, SE-60174 Norrköping, Sweden; Umeå Plant Science Centre, Department of Forest Genetics and Plant Physiology, Swedish University of Agricultural Sciences, SE-90183 Umeå, Sweden; [orcid.org/0000-0002-9357-776X](https://orcid.org/0000-0002-9357-776X); Email: [eleni.stavrinidou@liu.se](mailto:eleni.stavrinidou@liu.se)

### Authors

Cyril Routier – Laboratory of Organic Electronics, Department of Science and Technology, Linköping University, SE-60174 Norrköping, Sweden

Lorenzo Vallan – Laboratoire de Chimie des Polymères Organiques (LCPO–UMR 5629), Université de Bordeaux, Bordeaux INP, CNRS, F-33607 Pessac, France; [orcid.org/0000-0001-5267-4849](https://orcid.org/0000-0001-5267-4849)

Yohann Daguerre – Umeå Plant Science Centre, Department of Forest Genetics and Plant Physiology, Swedish University of Agricultural Sciences, SE-90183 Umeå, Sweden

Marta Juvany – Umeå Plant Science Centre, Department of Forest Genetics and Plant Physiology, Swedish University of Agricultural Sciences, SE-90183 Umeå, Sweden

Emin Istif – Laboratoire de Chimie des Polymères Organiques (LCPO–UMR 5629), Université de Bordeaux, Bordeaux INP, CNRS, F-33607 Pessac, France

Daniele Mantione – Laboratoire de Chimie des Polymères Organiques (LCPO–UMR 5629), Université de Bordeaux, Bordeaux INP, CNRS, F-33607 Pessac, France; POLYMAT, University of the Basque Country UPV/EHU, 20018 San Sebastián, Spain

Cyril Brochon – Laboratoire de Chimie des Polymères Organiques (LCPO–UMR 5629), Université de Bordeaux, Bordeaux INP, CNRS, F-33607 Pessac, France; [orcid.org/0000-0003-3242-1574](https://orcid.org/0000-0003-3242-1574)

Georges Hadziioannou – Laboratoire de Chimie des Polymères Organiques (LCPO–UMR 5629), Université de Bordeaux, Bordeaux INP, CNRS, F-33607 Pessac, France; [orcid.org/0000-0002-7377-6040](https://orcid.org/0000-0002-7377-6040)

Åsa Strand – Umeå Plant Science Centre, Department of Plant Physiology, Umeå University, SE 901-87 Umeå, Sweden

Torgny Näsholm – Umeå Plant Science Centre, Department of Forest Genetics and Plant Physiology, Swedish University of Agricultural Sciences, SE-90183 Umeå, Sweden

Eric Cloutet – Laboratoire de Chimie des Polymères Organiques (LCPO–UMR 5629), Université de Bordeaux, Bordeaux INP, CNRS, F-33607 Pessac, France

Eleni Pavlopoulou – Laboratoire de Chimie des Polymères Organiques (LCPO–UMR 5629), Université de Bordeaux, Bordeaux INP, CNRS, F-33607 Pessac, France; Institute of Electronic Structure and Laser, Foundation for Research and Technology—Hellas, 71110 Heraklion Crete, Greece; [orcid.org/0000-0002-5291-0132](https://orcid.org/0000-0002-5291-0132)

Complete contact information is available at: <https://pubs.acs.org/10.1021/acsnano.2c09255>

### Notes

The authors declare no competing financial interest.

## ACKNOWLEDGMENTS

This work was supported by the European Union's Horizon 2020 research and innovation program under Grant Agreement No. 800926 (FET-OPEN-HyPhOE) and by the Swedish Research Council (VR-2017-04910). Additional funding was provided by the Swedish Government Strategic Research Area in Materials Science on Advanced Functional Materials at Linköping University (Faculty Grant SFO-Mat-LiU No. 2009-00971). and by the European Union (ERC-2021-STG, 4DPhytoHybrid, 101042148). D.M. acknowledges funding from Ayuda RYC2021-031668-I financiada por MCIN/AEI/10.13039/501100011033 y por la Unión Europea NextGenerationEU/PRTR. Swedish Metabolomics Centre, Umeå, Sweden ([www.swedishmetabolomicscentre.se](http://www.swedishmetabolomicscentre.se)) is acknowledged for the LC-MS determination of 3-phosphoglyceric acid. The authors acknowledge the facilities and technical assistance of the Umeå Core Facility Electron Microscopy (UCEM) at the Chemical Biological Centre (KBC), Umeå University, a part of the National Microscopy Infrastructure NMI (VR-RFI 2019-00217). The authors thank Dr. C. Hermida-Carrera from the Department of Plant Physiology, Umeå Plant Science Centre, Sweden, for the assistance in establishing the assimilation-CO<sub>2</sub> response curves (A-Ci).

## REFERENCES

- (1) Martin, W.; Scheibe, R.; Schnarrenberger, C. The Calvin Cycle and Its Regulation. In *Photosynthesis. Advances in Photosynthesis and Respiration*; Leegood, R. C., Sharkey, T. D., von Caemmerer, S., Eds.; Springer: Dordrecht, 2000; Vol. 9, pp 9–51.
- (2) Raines, C. A. The Calvin Cycle Revisited. *Photosynth. Res.* **2003**, *75*, 1–10.
- (3) Sharkey, T. D. Estimating the Rate of Photorespiration in Leaves. *Physiol. Plant.* **1988**, *73*, 147–152.
- (4) Shi, X.; Bloom, A. Photorespiration: The Futile Cycle? *Plants* **2021**, *10*, 908.
- (5) Borovsky, D.; Smith, E. E.; Whelan, W. J. Purification and Properties of Potato 1,4-Alpha-d-Glucan: 1,4-Alpha-d-Glucan 6-Alpha-(1,4-Alpha-Glucano)-Transferase. Evidence against a Dual Catalytic Function in Amylose-Branching Enzyme. *Eur. J. Biochem.* **1975**, *59*, 615–625.
- (6) Kaldenhoff, R. Mechanisms Underlying CO<sub>2</sub> Diffusion in Leaves. *Curr. Opin. Plant Biol.* **2012**, *15*, 276–281.
- (7) Martin-Avila, E.; Lim, Y.-L.; Birch, R.; Dirk, L. M. A.; Buck, S.; Rhodes, T.; Sharwood, R. E.; Kapralov, M. v.; Whitney, S. M. Modifying Plant Photosynthesis and Growth via Simultaneous Chloroplast Transformation of Rubisco Large and Small Subunits. *Plant Cell* **2020**, *32*, 2898–2916.
- (8) Aigner, H.; Wilson, R. H.; Bracher, A.; Calisse, L.; Bhat, J. Y.; Hartl, F. U.; Hayer-Hartl, M. Plant RuBisCo Assembly in E. Coli with Five Chloroplast Chaperones Including BSD2. *Science* **2017**, *358*, 1272–1278.
- (9) Lin, M. T.; Stone, W. D.; Chaudhari, V.; Hanson, M. R. Small Subunits Can Determine Enzyme Kinetics of Tobacco Rubisco Expressed in Escherichia Coli. *Nat. Plants* **2020**, *6*, 1289–1299.
- (10) Whitney, S. M.; Houtz, R. L.; Alonso, H. Advancing Our Understanding and Capacity to Engineer Nature's CO<sub>2</sub>-Sequestering Enzyme, Rubisco. *Plant Physiol.* **2011**, *155*, 27–35.
- (11) Sharwood, R. E. Engineering Chloroplasts to Improve Rubisco Catalysis: Prospects for Translating Improvements into Food and Fiber Crops. *New Phytol* **2017**, *213*, 494–510.
- (12) Hanson, M. R.; Lin, M. T.; Carmo-Silva, A. E.; Parry, M. A. J. Towards Engineering Carboxysomes into C3 Plants. *Plant J.* **2016**, *87*, 38–50.
- (13) von Caemmerer, S.; Quick, W. P.; Furbank, R. T. The Development of C 4 Rice: Current Progress and Future Challenges. *Science* **2012**, *336*, 1671–1672.

- (14) Bar-Even, A.; Noor, E.; Lewis, N. E.; Milo, R. Design and Analysis of Synthetic Carbon Fixation Pathways. *Proc. Natl. Acad. Sci. U. S. A.* **2010**, *107*, 8889–8894.
- (15) Furbank, R. T.; Quick, W. P.; Sirault, X. R. R. Improving Photosynthesis and Yield Potential in Cereal Crops by Targeted Genetic Manipulation: Prospects, Progress and Challenges. *Field Crops Res.* **2015**, *182*, 19–29.
- (16) Buriak, J. M.; Liz-Marzán, L. M.; Parak, W. J.; Chen, X. Nano and Plants. *ACS Nano* **2022**, *16*, 1681–1684.
- (17) Dufil, G.; Bernacka-Wojcik, I.; Armada-Moreira, A.; Stavrinidou, E. Plant Bioelectronics and Biohybrids: The Growing Contribution of Organic Electronic and Carbon-Based Materials. *Chem. Rev.* **2022**, *122*, 4847–4883.
- (18) Lew, T. T. S.; Koman, V. B.; Gordiichuk, P.; Park, M.; Strano, M. S. The Emergence of Plant Nanobionics and Living Plants as Technology. *Adv. Mater. Technol.* **2020**, *5*, 1900657.
- (19) Lew, T. T. S.; Koman, V. B.; Silmore, K. S.; Seo, J. S.; Gordiichuk, P.; Kwak, S. Y.; Park, M.; Ang, M. C. Y.; Khong, D. T.; Lee, M. A.; Chan-Park, M. B.; Chua, N. H.; Strano, M. S. Real-Time Detection of Wound-Induced H<sub>2</sub>O<sub>2</sub> Signalling Waves in Plants with Optical Nanosensors. *Nat. Plants* **2020**, *6*, 404–415.
- (20) Lew, T. T. S.; Park, M.; Cui, J.; Strano, M. S. Plant Nanobionic Sensors for Arsenic Detection. *Adv. Mater.* **2021**, *33*, 2005683.
- (21) Santana, I.; Wu, H.; Hu, P.; Giraldo, J. P. Targeted Delivery of Nanomaterials with Chemical Cargoes in Plants Enabled by a Biorecognition Motif. *Nat. Commun.* **2020**, *11*, 2045.
- (22) Tullii, G.; Gobbo, F.; Costa, A.; Antognazza, M. R. A Prototypical Conjugated Polymer Regulating Signaling in Plants. *Adv. Sustain Syst.* **2022**, *6*, 2100048.
- (23) Stavrinidou, E.; Gabriëlsson, R.; Nilsson, K. P. R.; Singh, S. K.; Franco-Gonzalez, J. F.; Volkov, A. v.; Jonsson, M. P.; Grimoldi, A.; Elgland, M.; Zozoulenko, I. v.; Simon, D. T.; Berggren, M. In Vivo Polymerization and Manufacturing of Wires and Supercapacitors in Plants. *Proc. Natl. Acad. Sci. U. S. A.* **2017**, *114*, 2807–2812.
- (24) Dufil, G.; Parker, D.; Gerasimov, J. Y.; Nguyen, T.-Q.; Berggren, M.; Stavrinidou, E. Enzyme-Assisted in Vivo Polymerisation of Conjugated Oligomer Based Conductors. *J. Mater. Chem. B* **2020**, *8*, 4221–4227.
- (25) Parker, D.; Daguere, Y.; Dufil, G.; Mantione, D.; Solano, E.; Cloutet, E.; Hadziioannou, G.; Näsholm, T.; Berggren, M.; Pavlopoulou, E.; Stavrinidou, E. Biohybrid Plants with Electronic Roots via in Vivo Polymerization of Conjugated Oligomers. *Mater. Horiz.* **2021**, *8*, 3295–3305.
- (26) Giraldo, J. P.; Landry, M. P.; Faltermeier, S. M.; McNicholas, T. P.; Iverson, N. M.; Boghossian, A. A.; Reuel, N. F.; Hilmer, A. J.; Sen, F.; Brew, J. A.; Strano, M. S. Plant nanobionics approach to augment photosynthesis and biochemical sensing. *Nature Mater.* **2014**, *13*, 400–408.
- (27) Chandra, S.; Pradhan, S.; Mitra, S.; Patra, P.; Bhattacharya, A.; Pramanik, P.; Goswami, A. High Throughput Electron Transfer from Carbon Dots to Chloroplast: A Rationale of Enhanced Photosynthesis. *Nanoscale* **2014**, *6*, 3647–3655.
- (28) Xu, X.; Mao, X.; Zhuang, J.; Lei, B.; Li, Y.; Li, W.; Zhang, X.; Hu, C.; Fang, Y.; Liu, Y. PVA-Coated Fluorescent Carbon Dot Nanocapsules as an Optical Amplifier for Enhanced Photosynthesis of Lettuce. *ACS Sustain. Chem. Eng.* **2020**, *8*, 3938–3949.
- (29) Sai, L.; Liu, S.; Qian, X.; Yu, Y.; Xu, X. Nontoxic Fluorescent Carbon Nanodot Serving as a Light Conversion Material in Plant for UV Light Utilization. *Colloids Surf. B Biointerfaces* **2018**, *169*, 422–428.
- (30) Shen, X.; Du, H.; Mullins, R. H.; Kommalapati, R. R. Polyethyleneimine Applications in Carbon Dioxide Capture and Separation: From Theoretical Study to Experimental Work. *Energy Technol.* **2017**, *5*, 822–833.
- (31) Min, K.; Choi, W.; Kim, C.; Choi, M. Oxidation-Stable Amine-Containing Adsorbents for Carbon Dioxide Capture. *Nat. Commun.* **2018**, *9*, 726.
- (32) Xu, X.; Song, C.; Andresen, J. M.; Miller, B. G.; Scaroni, A. W. Novel Polyethyleneimine-Modified Mesoporous Molecular Sieve of MCM-41 Type as High-Capacity Adsorbent for CO<sub>2</sub> Capture. *Energy Fuels* **2002**, *16*, 1463–1469.
- (33) Zolghadrnasab, M.; Mousavi, A.; Farman, A.; Arpanaei, A. Ultrasound-Mediated Gene Delivery into Suspended Plant Cells Using Polyethyleneimine-Coated Mesoporous Silica Nanoparticles. *Ultrason. Sonochem.* **2021**, *73*, 105507.
- (34) Li, Y.; Cui, H. X.; Song, Y.; Li, Y.; Huang, J. li. Transient Expression of Exogenous Gene into Plant Cell Mediated by PEI Nanovector. *Agric. Sci. China* **2011**, *10*, 820–826.
- (35) Zhang, J.; Lei, W.; Meng, Y.; Zhou, C.; Zhang, B.; Yuan, J.; Wang, M.; Xu, D.; Meng, X.; Chen, W. Expression of PEI-Coated Gold Nanoparticles Carrying Exogenous Gene in Periwinkle Mesophyll Cells and Its Practice in Huanglongbing Research. *iScience* **2022**, *25*, 104479.
- (36) Zhang, H.; Cao, Y.; Xu, D.; Goh, N. S.; Demirel, G. S.; Cestellos-Blanco, S.; Chen, Y.; Landry, M. P.; Yang, P. Gold-Nanocluster-Mediated Delivery of siRNA to Intact Plant Cells for Efficient Gene Knockdown. *Nano Lett.* **2021**, *21*, 5859–5866.
- (37) Yasumoto, K.; Sakata, T.; Yasumoto, J.; Yasumoto-Hirose, M.; Sato, S. I.; Mori-Yasumoto, K.; Jimbo, M.; Kusumi, T.; Watabe, S. Atmospheric CO<sub>2</sub> Captured by Biogenic Polyamines Is Transferred as a Possible Substrate to Rubisco for the Carboxylation Reaction. *Sci. Rep.* **2018**, *8*, 17724.
- (38) Rychter, P.; Christova, D.; Lewicka, K.; Rogacz, D. Ecotoxicological Impact of Selected Polyethylenimines toward Their Potential Application as Nitrogen Fertilizers with Prolonged Activity. *Chemosphere* **2019**, *226*, 800–808.
- (39) Liu, Y.; Wenning, L.; Lynch, M.; Reineke, T. M. New Poly(D-Glucaramidoamine)s Induce DNA Nanoparticle Formation and Efficient Gene Delivery into Mammalian Cells. *J. Am. Chem. Soc.* **2004**, *126*, 7422–7423.
- (40) Smith, A. E.; Sizovs, A.; Grandinetti, G.; Xue, L.; Reineke, T. M. Diblock Glycopolymers Promote Colloidal Stability of Polyplexes and Effective PDNA and siRNA Delivery under Physiological Salt and Serum Conditions. *Biomacromolecules* **2011**, *12*, 3015–3022.
- (41) van Bruggen, C.; Hexum, J. K.; Tan, Z.; Dalal, R. J.; Reineke, T. M. Nonviral Gene Delivery with Cationic Glycopolymers. *Acc. Chem. Res.* **2019**, *52*, 1347–1358.
- (42) Oladzadabbasabadi, N.; Mohammadi Nafchi, A.; Ariffin, F.; Wijekoon, M. M. J. O.; Al-Hassan, A. A.; Dheyab, M. A.; Ghasemlou, M. Recent Advances in Extraction, Modification, and Application of Chitosan in Packaging Industry. *Carbohydr. Polym.* **2022**, *277*, 118876.
- (43) Cao, Y.; Tan, Y. F.; Wong, Y. S.; Liew, M. W. J.; Venkatraman, S. Recent Advances in Chitosan-Based Carriers for Gene Delivery. *Mar. Drugs* **2019**, *17*, 381.
- (44) Acet, Ö.; Baran, T.; Erdönmez, D.; Aksoy, N. H.; Alacabey, İ.; Menteş, A.; Odabaşı, M. O-Carboxymethyl Chitosan Schiff Base Complexes as Affinity Ligands for Immobilized Metal-Ion Affinity Chromatography of Lysozyme. *J. Chromatogr. A* **2018**, *1550*, 21–27.
- (45) Olivera, S.; Muralidhara, H. B.; Venkatesh, K.; Guna, V. K.; Gopalakrishna, K.; Kumar, K. Y. Potential Applications of Cellulose and Chitosan Nanoparticles/Composites in Wastewater Treatment: A Review. *Carbohydr. Polym.* **2016**, *153*, 600–618.
- (46) Malerba, M.; Cerana, R. Chitosan Effects on Plant Systems. *Int. J. Mol. Sci.* **2016**, *17*, 996.
- (47) Li, R.; He, J.; Xie, H.; Wang, W.; Bose, S. K.; Sun, Y.; Hu, J.; Yin, H. Effects of Chitosan Nanoparticles on Seed Germination and Seedling Growth of Wheat (*Triticum Aestivum* L.). *Int. J. Biol. Macromol.* **2019**, *126*, 91–100.
- (48) Joshi, H.; Rajawat, K.; Choudhary, J. Controlled Release Action of Chitosan Nanoparticles to Improve Nutrient Use Efficiency. *Int. J. Res. Agron.* **2020**, *3*, 36–41.
- (49) Khayrova, A.; Lopatin, S.; Shagdarova, B.; Sinitsyna, O.; Sinitsyn, A.; Varlamov, V. Evaluation of Antibacterial and Antifungal Properties of Low Molecular Weight Chitosan Extracted from *Hermetia Illucens* Relative to Crab Chitosan. *Molecules* **2022**, *27*, 577.
- (50) Moussa, A.; Crépet, A.; Ladavière, C.; Trombotto, S. Reducing-End “Clickable” Functionalizations of Chitosan Oligomers for the

Synthesis of Chitosan-Based Diblock Copolymers. *Carbohydr. Polym.* **2019**, *219*, 387–394.

(51) Fernandes Queiroz, M.; Melo, K.; Sabry, D.; Sasaki, G.; Rocha, H. Does the Use of Chitosan Contribute to Oxalate Kidney Stone Formation? *Mar. Drugs* **2015**, *13*, 141–158.

(52) Norkunas, K.; Harding, R.; Dale, J.; Dugdale, B. Improving Agroinfiltration-Based Transient Gene Expression in *Nicotiana Benthamiana*. *Plant Methods* **2018**, *14*, 71.

(53) Goodin, M. M.; Dietzgen, R. G.; Schichnes, D.; Ruzin, S.; Jackson, A. O. PGD Vectors: Versatile Tools for the Expression of Green and Red Fluorescent Protein Fusions in Agroinfiltrated Plant Leaves. *Plant J.* **2002**, *31*, 375–383.

(54) Liu, Z. Z.; Wang, J. L.; Huang, X.; Xu, W. H.; Liu, Z. M.; Fang, R. X. The Promoter of a Rice Glycine-Rich Protein Gene, *Osgrp-2*, Confers Vascular-Specific Expression in Transgenic Plants. *Planta* **2003**, *216*, 824–833.

(55) González-Grandío, E.; Demirer, G. S.; Jackson, C. T.; Yang, D.; Ebert, S.; Molawi, K.; Keller, H.; Landry, M. P. Carbon Nanotube Biocompatibility in Plants Is Determined by Their Surface Chemistry. *J. Nanobiotechnology* **2021**, *19*, 431.

(56) Sjöback, R.; Nygren, J.; Kubista, M. Absorption and Fluorescence Properties of Fluorescein. *Spectrochim. Acta, Part A* **1995**, *51*, 7–21.

(57) Tommasi, I. C. The Mechanism of Rubisco Catalyzed Carboxylation Reaction: Chemical Aspects Involving Acid-Base Chemistry and Functioning of the Molecular Machine. *Catalysts* **2021**, *11*, 813.

(58) Wong, M. H.; Misra, R. P.; Giraldo, J. P.; Kwak, S. Y.; Son, Y.; Landry, M. P.; Swan, J. W.; Blankschtein, D.; Strano, M. S. Lipid Exchange Envelope Penetration (LEEP) of Nanoparticles for Plant Engineering: A Universal Localization Mechanism. *Nano Lett.* **2016**, *16*, 1161–1172.

(59) Floryszak-Wieczorek, J.; Arasimowicz-Jelonek, M. The Multifunctional Face of Plant Carbonic Anhydrase. *Plant Physiol. Biochem.* **2017**, *12*, 362–368.

(60) DiMario, R. J.; Clayton, H.; Mukherjee, A.; Ludwig, M.; Moroney, J. v. Plant Carbonic Anhydrases: Structures, Locations, Evolution, and Physiological Roles. *Mol. Plant* **2017**, *10*, 30–46.

(61) Chincinska, I. A. Leaf Infiltration in Plant Science: Old Method, New Possibilities. *Plant Methods* **2021**, *17*, 83.

(62) Koman, V. B.; Park, M.; Lew, T. T. S.; Wan, S.; Yarwood, E. S.; Gong, X.; Shikdar, T. S.; Oliver, R. J.; Cui, J.; Gordiichuk, P.; Sarojam, R.; Strano, M. S. Emerging Investigator Series: Linking Nanoparticle Infiltration and Stomatal Dynamics for Plant Nanobionics. *Environ. Sci. Nano* **2022**, *9*, 1236–1246.

## Recommended by ACS

### Determination of 2D Particle Size Distributions in Plasmonic Nanoparticle Colloids via Analytical Ultracentrifugation: Application to Gold Bipyramids

Uwe Frank, Wolfgang Peukert, *et al.*

MARCH 15, 2023  
ACS NANO

[READ](#)

### Chiral Nanosilica Drug Delivery Systems Stereoselectively Interacted with the Intestinal Mucosa to Improve the Oral Adsorption of Insoluble Drugs

Xuchun Chen, Heran Li, *et al.*

FEBRUARY 14, 2023  
ACS NANO

[READ](#)

### Toward High-Performance Green Piezoelectric Generators Based on Electrochemically Poled Nanocellulose

Ayesha Sultana, Dan Zhao, *et al.*

FEBRUARY 03, 2023  
CHEMISTRY OF MATERIALS

[READ](#)

### Foodborne Carbon Dot Exposure Induces Insulin Resistance through Gut Microbiota Dysbiosis and Damaged Intestinal Mucus Layer

Boya Zhang, Ning Gu, *et al.*

MARCH 10, 2023  
ACS NANO

[READ](#)

[Get More Suggestions >](#)